

# Integrability of Kerr-Newman spacetime with cloud strings, quintessence and electromagnetic field

Wenfu Cao<sup>1,2</sup>, Wenfang Liu<sup>1</sup>, and Xin Wu<sup>1,2,3\*</sup>

*School of Mathematics, Physics and Statistics, Shanghai University of Engineering Science, Shanghai 201620, China*

*<sup>2</sup>Center of Application and Research of Computational Physics,*

*Shanghai University of Engineering Science, Shanghai 201620, China*

*<sup>3</sup>Guangxi Key Laboratory for Relativistic Astrophysics, Guangxi University, Nanning 530004, China*

The dynamics of charged particles moving around a Kerr-Newman black hole surrounded by cloud strings, quintessence and electromagnetic field is integrable due to the presence of a fourth constant of motion like the Carter constant. The fourth motion constant and the axial-symmetry of the spacetime give a chance to the existence of radial effective potentials with stable circular orbits in two-dimensional planes, such as the equatorial plane and other nonequatorial planes. They also give a possibility of the presence of radial effective potentials with stable spherical orbits in the three-dimensional space. The dynamical parameters play important roles in changing the graphs of the effective potentials. In addition, variations of these parameters affect the presence or absence of stable circular orbits, innermost stable circular orbits, stable spherical orbits and marginally stable spherical orbits. They also affect the radii of the stable circular or spherical orbits. It is numerically shown that the stable circular orbits and innermost stable circular orbits can exist not only in the equatorial plane but also in the nonequatorial planes. Several stable spherical orbits and marginally stable spherical orbits are numerically confirmed, too. In particular, there are some stable spherical orbits and marginally stable spherical orbits with vanishing angular momenta for covering whole the range of the latitudinal coordinate.

PACS numbers:

## I. INTRODUCTION

Cosmological observations such as the cosmic microwave background thermal anisotropies support the accelerating expansion of the Universe [1]. The expansion is well explained by a dark energy with repulsive gravitational effect. The dark energy is dependent on the cosmological constant and the so-called quintessence surrounding a black hole [2]. The cosmological constant acting as vacuum energy with negative pressure causes the acceleration. The quintessence as a scalar field coupled to gravity has negative pressure. The quintessence plays a role in the cosmological constant for an appropriate choice of the quintessence parameters [2]. The Robertson-Walker metric with the accelerating scale factor caused by the quintessence and the Reissner-Nordström-de Sitter black hole surrounded by the quintessence can be found in [2,3]. The importance of quintessential fields in the physical processes occurring around black holes has been discussed in [4-7].

In addition to the quintessence, another extra source representing the universe is not a collection of point particles, but is a collection of extended objects, such as one-dimensional strings considered by Letelier [8]. These extended objects like a cloud of strings surrounding a black hole are helpful to describe physical phenomena in the universe, and have astrophysical observable consequences [9]. A static and spherically symmetric black

hole surrounded by the quintessence and the cloud of strings was given in [10]. The Reissner-Nordström metric with the quintessence and the cloud of strings was also obtained in [11].

With the aid of the Newman-Janis algorithm [12], the above-mentioned non-rotating black holes with the quintessence and/or the cloud of strings can be transformed to rotating black hole counterparts [13-16]. Adding the cosmological constant, the authors of [17] obtained the Kerr-Newman-AdS solutions of the Einstein-Maxwell equation in quintessence field. Toledo & Bezerra [18] studied the Kerr-Newman-AdS black hole with quintessence and cloud of strings. In this case, the electromagnetic potential is generated due to the charge in the black hole.

If these extra perturbation sources like the quintessence, cloud of strings and electromagnetic fields are not considered, the Schwarzschild, Reissner-Nordström metric, Kerr and Kerr-Newman metrics are integrable. As far as the axially-symmetric Kerr spacetime is concerned, it is integrable due to four constants of motion, which are the particle (or photon) energy, angular momentum and rest mass associated with the 4-velocity normalizing condition and the Carter constant governing the motion of geodesics in the latitudinal direction [19]. The existence of the Carter constant as the fourth constant gives the Kerr spacetime the possibility of non-planar orbits with constant coordinate radii corresponding to spherical photon orbits [20,21] as well as the existence of circular orbits in the equatorial plane. Wilkins [22] first found the existence of unstable spherical photon orbits around the Kerr black hole

---

\*Electronic address: xinwu@gxu.edu.cn, wuxin'1134@sina.com

and studied many properties of the spherical photon orbits. This result was extended to spherical orbits of charged particles in a Kerr-Newman geometry by Johnston and Ruffini [23]. Several numerical examples of spherical photon orbits around a Kerr black hole were plotted by Teo [20,24]. Exact formulas for spherical photon orbits around Kerr black holes were given by Tavlayan and Tekin [25]. The observability of a series of images produced by spherical photon orbits around near-extremal Kerr black holes was shown by Igata et al. [26]. The authors of [27] studied properties of spherical photon orbits in the Kerr naked singularity spacetimes. Spherical photon orbits were discussed in the field of Kerr-de Sitter black holes [28,29] and a five-dimensional rotating black hole [30]. The ringdown and shadow observables are relevant to a special set of unstable null orbits with constant radii. These orbits are light rings [31-36] for the spherically-symmetric Schwarzschild type black holes and spherical photon orbits for the axially-symmetric Kerr type spacetimes. The threshold spherical photon orbits mark a boundary between the photons captured by the black hole and the photons escaping to infinity. Therefore, there have been many other papers focusing on these spherical photon orbits (see, e.g., [37-39]).

When the quintessence and the cloud of strings as two extra perturbation sources are included, they do not destroy the integrability of the considered spacetimes. However, the fourth constant or the integrability becomes absent in most cases when electromagnetic fields as an external perturbation source are further included in these spacetimes. Even these external magnetic fields induce chaos of charged-particle motions under appropriate circumstances [40-48]. In spite of this, not all the external magnetic fields surrounding the black holes can eliminate the existence of the fourth constant. As Carter [19] claimed, not only the geodesic equations of particles (or photons) around the Kerr black hole but also the equations of charged-particle orbits in the Kerr spacetime with an electromagnetic field described by a covariant vector potential are analytically solved. Their solutions are expressed in terms of explicit quadratures. Although such a covariant vector potential is replaced with a more complicated form, the integrability of charged particle motions in Kerr-Newmann spacetimes was shown by Hackmann and Xu [49]. In other words, the fourth constant of motion is still existent.

Apart from the two Kerr type black holes with external magnetic fields mentioned in [19,49], the dynamics of charged particles moving around the Kerr-Newman black hole surrounded by cloud strings, quintessence and electromagnetic field [18] is integrable. Providing such an integrable example is the main motivation of the present paper. Based on this integrability, stable circular charged-particle orbits exist in two-dimensional planes, which are not confined to the equatorial plane. Stable spherical charged-particle orbits are also present. Unlike the authors who studied the spherical photon orbits in

the literature [37-39], we mainly focus on the stable circular charged-particle orbits in two-dimensional nonequatorial planes and the stable spherical charged-particle orbits. They are important in an astrophysical scenario. The structure of the thin accretion Keplerian disks is governed by the stable equatorial circular orbits of test particles [27]. Above all, the innermost stable circular orbits act as the inner boundary of the Keplerian disks. The threshold spherical charged-particle orbits are important to model the capture or accretion of matter by the black hole.

The outline of the paper is organized as follows. In Section II, we introduce the considered dynamical model. In Section III, we analyze the integrability of this system, radial effective potentials, circular orbits and spherical orbits of charged particles. Finally, we conclude our conclusions in Section IV.

## II. KERR-NEWMAN BLACK HOLE WITH EXTRA PERTURBATION SOURCES

The considered spacetime metric is introduced briefly. A super-Hamiltonian for describing the motion of charged particles around the Kerr-Newman black hole immersed in an external electromagnetic field is given.

### A. Description of spacetime metric

A negative pressure from a gravitationally repulsive energy component leads to the accelerated expansion of the universe. Its origin may be due to quintessence dark energy surrounding a black hole. In Boyer-Lindquist coordinates  $(t, r, \theta, \phi)$ , a spherically-symmetric static Schwarzschild black hole surrounded by the quintessence is expressed in [2] as

$$ds^2 = g_{\alpha\beta} dx^\alpha dx^\beta, \quad (1)$$

where covariant metric  $g_{\alpha\beta}$  has four nonzero components:

$$g_{tt} = -\left(1 - \frac{2M}{r} - \frac{\alpha_q}{r^{3\omega_q+1}}\right), \quad (2)$$

$$g_{rr} = \left(1 - \frac{2M}{r} - \frac{\alpha_q}{r^{3\omega_q+1}}\right)^{-1}, \quad (3)$$

$$g_{\theta\theta} = r^2, \quad (4)$$

$$g_{\phi\phi} = r^2 \sin^2 \theta. \quad (5)$$

$M$  is the black hole mass. The state equation describing the relation among the quintessential state parameter  $\omega_q$ , the pressure  $p_{quint}$  and the energy density  $\rho_{quint}$  is

$$p_{quint} = \omega_q \rho_{quint}, \quad (6)$$

$$\rho_{quint} = -\frac{3}{2} \frac{\alpha_q \omega_q}{r^{3(\omega_q+1)}}. \quad (7)$$

$\alpha_q \neq 0$  is a quintessence parameter, and  $\alpha_q = 0$  corresponds to the Schwarzschild black hole. If  $\rho_{quint} > 0$ ,

then  $\alpha_q \omega_q < 0$ . The parameter  $\alpha_q$  is positive for the quintessence field. Thus, the quintessential state parameter  $\omega_q$  is negative. The state parameter has three cases [7,16]:  $-1 < \omega_q < -1/3$  for the quintessence,  $\omega_q < -1$  for the phantom energy, and  $\omega_q = -1$  acting as a cosmological constant. The quintessence corresponds to the stress-energy tensors

$$T_t^t = T_r^r = \rho_{quint}, \quad (8)$$

$$T_\theta^\theta = T_\phi^\phi = -\frac{\rho_{quint}}{2}(3\omega_q + 1). \quad (9)$$

The properties of quintessence in an astrophysical scenario have been discussed in some literature [4-7].

Letelier [8] considered the Schwarzschild black hole surrounded by another extra source, which is a spherically-symmetric cloud of strings as a collection of extended objects instead of point particles. In this case, the stress-energy tensors are

$$T_t^t = T_r^r = \rho_{cloud} = \frac{b_c}{r^2}, \quad (10)$$

$$T_\theta^\theta = T_\phi^\phi = 0, \quad (11)$$

where  $\rho_{cloud}$  represents the energy density regarding the string cloud and  $b_c$  is a positive parameter measuring the intensity of the cloud of strings. Replacing the quintessence term in Eqs. (2) and (3) with the string cloud intensity  $b_c$ , Letelier obtained two metric components of the Schwarzschild black hole with the string cloud as follows:

$$g_{tt} = -(1 - \frac{2M}{r} - b_c), \quad (12)$$

$$g_{rr} = (1 - \frac{2M}{r} - b_c)^{-1}. \quad (13)$$

When the quintessence and the cloud of strings as two extra sources of energy surround the Schwarzschild black hole, the total stress-energy tensor is a linear combination of the stress-energy tensors corresponding to the quintessence and the one associated with the cloud of strings:

$$\begin{aligned} T_t^t &= T_r^r = \rho_{quint} + \rho_{cloud} \\ &= \frac{b_c}{r^2} - \frac{3}{2} \frac{\alpha_q \omega_q}{r^{3(\omega_q+1)}}, \end{aligned} \quad (14)$$

$$T_\theta^\theta = T_\phi^\phi = -\frac{\rho_{quint}}{2}(3\omega_q + 1). \quad (15)$$

Based on Eqs. (2), (3), (12) and (13), two components of the metric for the description of the Schwarzschild black hole surrounded by the quintessence and the cloud of strings can be written in [10] as follows:

$$g_{tt} = -(1 - b_c - \frac{2M}{r} - \frac{\alpha_q}{r^{3\omega_q+1}}), \quad (16)$$

$$g_{rr} = (1 - b_c - \frac{2M}{r} - \frac{\alpha_q}{r^{3\omega_q+1}})^{-1}. \quad (17)$$

Suppose the black hole has an electrical charge  $Q$  inducing an electromagnetic field. The authors of [11] provided a metric for the Reissner-Nordström black hole surrounded by the quintessence and the cloud of strings. The two metric components  $g_{tt}$  and  $g_{rr}$  are

$$g_{tt} = -(1 - b_c - \frac{2M}{r} + \frac{Q^2}{r^2} - \frac{\alpha_q}{r^{3\omega_q+1}}), \quad (18)$$

$$g_{rr} = (1 - b_c - \frac{2M}{r} + \frac{Q^2}{r^2} - \frac{\alpha_q}{r^{3\omega_q+1}})^{-1}. \quad (19)$$

In terms of the Newman-Janis algorithm [12], the Reissner-Nordström black hole metric with the quintessence and the cloud of strings can be transformed into the Kerr-Newman black hole metric in the quintessence and the cloud of strings [13-16]. Adding a cosmological constant  $\Lambda$  [17], the authors of [18] obtained a Kerr-Newman-AdS solution immersed in quintessence and string cloud. The metric solution has six nonzero components [18]:

$$g_{tt} = \frac{1}{\Sigma \Xi^2} (\Delta_\theta a^2 \sin^2 \theta - \Delta_r), \quad (20)$$

$$g_{t\phi} = \frac{a \sin^2 \theta}{\Sigma \Xi^2} [\Delta_r - \Delta_\theta (r^2 + a^2)] = g_{\phi t}, \quad (21)$$

$$g_{rr} = \frac{\Sigma}{\Delta_r}, \quad (22)$$

$$g_{\theta\theta} = \frac{\Sigma}{\Delta_\theta}, \quad (23)$$

$$g_{\phi\phi} = \frac{\sin^2 \theta}{\Sigma \Xi^2} [\Delta_\theta (r^2 + a^2)^2 - \Delta_r a^2 \sin^2 \theta]. \quad (24)$$

The above notations are specified by

$$\Sigma = r^2 + a^2 \cos^2 \theta, \quad (25)$$

$$\begin{aligned} \Delta_r &= (1 - b_c) r^2 + a^2 + Q^2 - 2Mr \\ &\quad - \frac{\Lambda}{3} r^2 (r^2 + a^2) - \alpha_q r^{1-3\omega_q}, \end{aligned} \quad (26)$$

$$\Delta_\theta = 1 + \frac{\Lambda}{3} a^2 \cos^2 \theta, \quad (27)$$

$$\Xi = 1 + \frac{\Lambda}{3} a^2. \quad (28)$$

The angular momentum of the rotating black hole is given in the range  $a \in [-M, M]$ . The black hole's electrical charge is given in the range  $Q \in [-M, M]$ . The speed of light  $c$  and the gravitational constant  $G$  take geometrized units,  $c = G = 1$ .

## B. Super-Hamiltonian system

The charge in the Kerr-Newman-AdS black hole generates an electromagnetic potential [18]

$$A_\mu = -\frac{Qr}{\Sigma} \delta_\mu^t + \frac{Qra \sin^2 \theta}{\Sigma \Xi} \delta_\mu^\phi. \quad (29)$$

The motion of a test particle with charge  $q$  and mass  $m$  around the Kerr-Newman-AdS black hole surrounded with the quintessence, string cloud and electromagnetic field is governed by the super-Hamiltonian

$$\begin{aligned} H &= \frac{1}{2m} g^{\mu\nu} (p_\mu - qA_\mu)(p_\nu - qA_\nu) \\ &= \frac{1}{2m} g^{tt} (p_t - qA_t)^2 + \frac{1}{2m} g^{\phi\phi} (p_\phi - qA_\phi)^2 \\ &\quad + \frac{1}{m} g^{t\phi} (p_t - qA_t)(p_\phi - qA_\phi) + \frac{1}{2m} g^{rr} p_r^2 \\ &\quad + \frac{1}{2m} g^{\theta\theta} p_\theta^2, \end{aligned} \quad (30)$$

where the six non-zero covariant metric components (20)-(24) correspond to their contravariant components

$$g^{tt} = \frac{\Xi^2}{\Sigma} \left[ \frac{a^2}{\Delta_\theta} \sin^2 \theta - \frac{(r^2 + a^2)^2}{\Delta_r} \right], \quad (31)$$

$$g^{t\phi} = \frac{a\Xi^2}{\Sigma} \left( \frac{1}{\Delta_\theta} - \frac{r^2 + a^2}{\Delta_r} \right) = g_{\phi t}, \quad (32)$$

$$g^{rr} = \frac{\Delta_r}{\Sigma}, \quad (33)$$

$$g^{\theta\theta} = \frac{\Delta_\theta}{\Sigma}, \quad (34)$$

$$g^{\phi\phi} = \frac{\Xi^2}{\Sigma} \left( \frac{1}{\Delta_\theta \sin^2 \theta} - \frac{a^2}{\Delta_r} \right). \quad (35)$$

Considering a set of Hamiltonian canonical equations  $\dot{x}^\mu = \partial H / \partial p_\mu = g^{\mu\nu} (p_\nu - qA_\nu) / m$ , we have the covariant generalized momenta

$$p_\mu = m g_{\mu\nu} \dot{x}^\nu + qA_\mu. \quad (36)$$

Because another set of Hamiltonian canonical equations satisfy  $\dot{p}_t = -\partial H / \partial t = 0$  and  $\dot{p}_\phi = -\partial H / \partial \phi = 0$ ,  $p_t$  and  $p_\phi$  are two constants of motion.  $p_t$  corresponds to an energy of the particle, and  $p_\phi$  is an angular momentum of the particle. They are

$$E = -p_t = -[m(g_{tt}\dot{t} + g_{t\phi}\dot{\phi}) + qA_t], \quad (37)$$

$$L = p_\phi = m(g_{t\phi}\dot{t} + g_{\phi\phi}\dot{\phi}) + qA_\phi. \quad (38)$$

Dimensionless operations are given to Eq. (30). The distances, coordinate time  $t$  and  $a$  take the black hole mass  $M$  as units; that is,  $r \rightarrow rM$ ,  $t \rightarrow tM$  and  $a \rightarrow aM$ . The proper time  $\tau$  also takes the mass unit,  $\tau \rightarrow \tau M$ . In addition,  $Q \rightarrow QM$ ,  $\Lambda \rightarrow \Lambda/M^2$ ,  $\alpha_q \rightarrow \alpha_q M^{1+3\omega_q}$ ,  $H \rightarrow Hm$ ,  $E \rightarrow Em$ ,  $p_r \rightarrow p_r m$ ,  $p_\theta \rightarrow p_\theta Mm$ ,  $L \rightarrow LMm$ , and  $q \rightarrow qm$ . It is particularly pointed out that  $E$  and  $p_r$  are measured in terms of  $m$ , but  $p_\theta$  is measured in terms of  $mM$ . The particle's angular momentum  $L$  is also measured in terms of  $mM$ , whereas the black hole's angular momentum  $a$  is measured in terms of  $M$ . After the dimensionless operations are implemented,  $a \in [-1, 1]$ ,  $Q \in [-1, 1]$ , and  $-2Mr$  in Eq. (26) becomes  $-2r$ . The Hamiltonian (30) becomes a dimension-

less form

$$\begin{aligned} H &= \frac{1}{2} \frac{\Xi^2}{\Sigma} \left[ \frac{a^2}{\Delta_\theta} \sin^2 \theta - \frac{(r^2 + a^2)^2}{\Delta_r} \right] \left( \frac{Q^* r}{\Sigma} - E \right)^2 \\ &\quad + \frac{1}{2} \frac{\Xi^2}{\Sigma} \left( \frac{1}{\Delta_\theta \sin^2 \theta} - \frac{a^2}{\Delta_r} \right) \left( L - \frac{Q^* a r}{\Sigma \Xi} \sin^2 \theta \right)^2 \\ &\quad + \frac{a\Xi^2}{\Sigma} \left( \frac{1}{\Delta_\theta} - \frac{r^2 + a^2}{\Delta_r} \right) \left( L - \frac{Q^* a r}{\Sigma \Xi} \sin^2 \theta \right) \\ &\quad \cdot \left( \frac{Q^* r}{\Sigma} - E \right) + \frac{1}{2} \frac{\Delta_r}{\Sigma} p_r^2 + \frac{1}{2} \frac{\Delta_\theta}{\Sigma} p_\theta^2, \end{aligned} \quad (39)$$

where  $Q^* = qQ$  is an electromagnetic field parameter.

The Hamiltonian (39) is a relatively complicated 4-dimensional nonlinear system with two degrees of freedom  $r$  and  $\theta$ . For the time-like case, this Hamiltonian is always identical to a given constant

$$H = -\frac{1}{2}. \quad (40)$$

The existence of this constant is because the particle's 4-velocity  $\dot{x}^\mu = (\dot{t}, \dot{r}, \dot{\theta}, \dot{\phi}) = U^\mu = \partial H / \partial p_\mu = g^{\mu\nu} (p_\nu - qA_\nu)$  satisfies the relation  $U^\mu U_\mu = -1$  or the particle's rest mass is conserved.

### III. INTEGRABLE DYNAMICS OF CHARGED PARTICLES

Firstly, we discuss the integrability of the Hamiltonian system (39) with a vanishing cosmological constant by finding a fourth integral of motion in this system. Secondly, physically allowed motion regions are analyzed. Thirdly, radial effective potentials in two-dimensional planes are focused on and some stable circular orbits are given. Finally, radial effective potentials in the three-dimensional space are considered and some stable spherical orbits are obtained.

#### A. Integrability of the system (39) without cosmological constant

As is demonstrated above, the particle's energy  $E$ , angular momentum  $L$  and rest mass are three constants of motion in the system (39). Does a fourth constant exist? Yes, it does when  $\Lambda = 0$  although the magnetic field, cloud strings and quintessence field are included in the Kerr-Newman spacetime. In what follows, we introduce how to find the fourth constant.

Clearly,  $\Delta_\theta = \Xi = 1$  in the case of  $\Lambda = 0$ . The system

(39) satisfying Eq. (40) becomes

$$\begin{aligned}
-\Sigma &= [a^2 \sin^2 \theta - \frac{(r^2 + a^2)^2}{\Delta_r}] (\frac{Q^* r}{\Sigma} - E)^2 \\
&+ (\frac{1}{\sin^2 \theta} - \frac{a^2}{\Delta_r}) (L - \frac{Q^* a r}{\Sigma} \sin^2 \theta)^2 \\
&+ 2a(1 - \frac{r^2 + a^2}{\Delta_r}) (L - \frac{Q^* a r}{\Sigma} \sin^2 \theta) \\
&\cdot (\frac{Q^* r}{\Sigma} - E) + \Delta_r p_r^2 + p_\theta^2.
\end{aligned} \quad (41)$$

This equation has a separable variable form

$$\begin{aligned}
&\frac{1}{\Delta_r} [aL - E(r^2 + a^2) + Q^* r]^2 - r^2 - \Delta_r p_r^2 \\
&= (Ea \sin \theta - \frac{L}{\sin \theta})^2 + a^2 \cos^2 \theta + p_\theta^2.
\end{aligned} \quad (42)$$

The left-hand side of this equality is a function of  $r$ , but the right-hand side of this equality is another function of  $\theta$ . In general, the equality is impossible. If and only if both sides are equal to a new constant denoted by  $K$ , the equality (42) is admissible. This means that Eq. (42) can be split into two equations

$$\frac{1}{\Delta_r} [aL - E(r^2 + a^2) + Q^* r]^2 - r^2 - \Delta_r p_r^2 = K, \quad (43)$$

$$p_\theta^2 + (aE \sin \theta - \frac{L}{\sin \theta})^2 + a^2 \cos^2 \theta = K. \quad (44)$$

They belong to a first integral of motion similar to the Carter constant [19]. Eq. (43) or Eq. (44) is the fourth constant of motion in the system (39). In fact, the obtainment of the fourth constant or Eq. (42) implicitly comes from the Hamilton-Jacobi equation of the Hamiltonian (39).

The four independent constants are described by Eqs. (37), (38), (40) and (43) (or (44)). They determine the integrability of the system (39). If  $\Lambda \neq 0$ , then no separable form (42) exists, and Eqs. (43) and (44) do not exist, either. Thus, the system (39) is nonintegrable. Only the case of  $\Lambda = 0$  is considered in our later discussions.

## B. Physically allowed motion regions

Eqs. (43) and (44) are respectively rewritten as

$$\begin{aligned}
\Sigma^2 \dot{r}^2 &= [aL - E(r^2 + a^2) + Q^* r]^2 - (r^2 + K)\Delta_r \\
&= \mathfrak{R}(r).
\end{aligned} \quad (45)$$

$$\begin{aligned}
\Sigma^2 \dot{\theta}^2 &= K - a^2 \cos^2 \theta - (aE \sin \theta - \frac{L}{\sin \theta})^2 \\
&= K - a^2 + 2aEL + a^2(1 - E^2) \sin^2 \theta \\
&\quad - \frac{L^2}{\sin^2 \theta} = \Theta(\theta).
\end{aligned} \quad (46)$$

The conditions for physically allowed motions are

$$\mathfrak{R}(r) \geq 0 \quad (47)$$

$$\Theta(\theta) \geq 0. \quad (48)$$

Eq. (47) corresponds to  $E \geq E^+$  or  $E \leq E^-$ , where  $E^\pm$  are given by

$$E^\pm = (aL + Q^* r \pm \sqrt{(r^2 + K)\Delta_r}) / (r^2 + a^2). \quad (49)$$

In fact, their expressions are based on  $\mathfrak{R}(r) = 0$ . For  $|E| < 1$ ,  $r$  in Eq. (47) can be allowed in a finite range outside the event horizon; that is, the corresponding orbit is bound [22]. For  $|E| \geq 1$ ,  $r$  in Eq. (47) can be allowed in a semi-infinite range outside the event horizon; namely, the orbit is unbound.

The physically allowed ranges of parameters for Eq. (48) are given according to several cases. Because  $d\Theta/d\theta = 2 \cos \theta [a^2(1 - E^2) \sin \theta + L^2/\sin^3 \theta]$ , the function  $\Theta$  has a maximum at  $\theta = \pi/2$  for  $|E| < 1$  (precisely speaking,  $E^+ \leq E < 1$  or  $-1 < E \leq E^-$ ), i.e.,  $\Theta_{max} = K - (aE + L)^2$  with  $K \geq (aE + L)^2$ . In this case, we have  $\vartheta \leq \theta \leq \pi - \vartheta$ , where  $\vartheta$  is a positive root of the equation  $\Theta = 0$  as follows:

$$\begin{aligned}
\vartheta &= \arcsin\{(\sqrt{\varrho^2 + 4a^2(1 - E^2)L^2} - \varrho) \\
&\quad / [2a^2(1 - E^2)]\}^{\frac{1}{2}} \quad (|E| < 1 \text{ and } a \neq 0),
\end{aligned} \quad (50)$$

$$\vartheta = \arcsin(L/\sqrt{\varrho}) \quad (a = 0), \quad (51)$$

$$\varrho = K - a^2 + 2aEL > 0.$$

If  $|E| \geq 1$  (precisely speaking,  $E \geq \max\{E^+, 1\}$  or  $E \leq \min\{E^-, -1\}$ ), the function  $\Theta$  reaches a maximum at  $\theta = \psi$  or  $\theta = \pi - \psi$ , where  $\psi$  and the maximum are expressed as

$$\psi = \arcsin[\frac{L^2}{a^2(E^2 - 1)}]^{1/4} \quad (0 \leq L \leq a\sqrt{E^2 - 1}), \quad (52)$$

$$\Theta_{max} = K - a^2 + 2aL(E - \sqrt{E^2 - 1}). \quad (53)$$

The motions are confined to a region  $\theta \in (0, \zeta] \cup [\pi - \zeta, \pi)$ , where

$$\begin{aligned}
\zeta &= \arcsin\{(\sqrt{\varrho^2 + 4a^2(1 - E^2)L^2} + \varrho) \\
&\quad / [2a^2(E^2 - 1)]\}^{\frac{1}{2}} \quad (a \neq 0, |E| \neq 1).
\end{aligned} \quad (54)$$

Thus, the motions for these cases are always confined to the region  $\theta \in [\vartheta, \pi - \vartheta]$  or  $\theta \in (0, \zeta] \cup [\pi - \zeta, \pi)$ .

In particular, the conditions for the orbits covering whole the range of the latitudinal coordinate  $\theta \in (0, \pi)$  (note that 0 and  $\pi$  are coordinate singularities) and reaching the symmetry axis at  $\theta = 0$  can be found from Eq. (48) or the physically allowed ranges of  $\theta$ . The conditions for  $\theta \in (0, \pi)$  are one of the following two cases. (i)  $L = 0$ ,  $|E| < 1$  and  $K \geq a^2 \geq 0$ . (ii)  $L = 0$ ,  $|E| \geq 1$  and  $K \geq a^2 E^2 \geq 0$ . It is clear that zero angular momentum  $L = 0$  is a necessary condition for the orbits covering whole the range of the latitudinal coordinate.



### C. Effective potentials and stable circular orbits in two-dimensional planes

Based on  $\Theta = 0$  with  $\theta = \pi/2$ , the fourth constant  $K$  is given by

$$K = a^2 - 2aLE^\pm - a^2[1 - (E^\pm)^2] + L^2. \quad (55)$$

In this case,  $E^\pm$  are the standard radial effective potentials at the equatorial plane  $\theta = \pi/2$  in many references (e.g., [31-36]). Solving Eqs. (49) and (55) (or Eq. (42) with  $\theta = \pi/2$ ), we have the energies

$$\begin{aligned} V_{\pi/2}^\pm &= \frac{-B \pm \sqrt{B^2 - AC}}{A}, \\ A &= (r^2 + a^2)^2 - a^2\Delta_r, \\ B &= aL\Delta_r - (aL + Q^*r)(r^2 + a^2), \\ C &= (aL + Q^*r)^2 - (r^2 + L^2)\Delta_r. \end{aligned} \quad (56)$$

The radial effective potentials  $V_{\pi/2}^\pm$  at the equatorial plane  $\theta = \pi/2$  depend on separation  $r$  and parameters  $a$ ,  $L$ ,  $Q$ ,  $Q^*$ ,  $b_c$ ,  $\alpha_q$  and  $\omega_q$ .

Besides the radial effective potentials in the equatorial plane, they are present in other planes. The planes are determined by  $\Theta(\theta) = 0$  corresponding to  $\dot{\theta} = 0$  in Eq. (46) and can be described by  $\theta = \sigma$ . Here,  $\sigma$  is a parameter describing some plane. In this case,  $K$  reads

$$K = (aE \sin \sigma - \frac{L}{\sin \sigma})^2 + a^2 \cos^2 \sigma. \quad (57)$$

The energies obtained from Eqs. (43) and (57) are expressed as

$$\begin{aligned} V_\sigma^\pm &= \frac{-B \pm \sqrt{B^2 - A_\sigma C_\sigma}}{A_\sigma}, \\ A_\sigma &= (r^2 + a^2)^2 - a^2\Delta_r \sin^2 \sigma, \\ C_\sigma &= (aL + Q^*r)^2 - (r^2 + \frac{L^2}{\sin^2 \sigma} + a^2 \cos^2 \sigma)\Delta_r. \end{aligned} \quad (58)$$

Eq. (58) is the radial effective potentials in the plane  $\theta = \sigma$  and includes the results in Eq. (56). Such radial effective potentials in the nonequatorial planes are seldom met in the existing literature.

Without loss of generality,  $V_\sigma^+$  is considered. The local extrema of the effective potentials  $V_\sigma^+$  correspond to circular orbits with constant radii  $r$ , which satisfy the conditions

$$\Theta(\theta) = 0, \quad \frac{dV_\sigma^+}{dr} = 0. \quad (59)$$

The local minima of the effective potentials  $V_\sigma^+$  represent stable circular orbits (SCOs), which satisfy Eq. (59) and the following condition

$$\frac{d^2 V_\sigma^+}{dr^2} \geq 0. \quad (60)$$

The equality symbol “=” indicates the innermost stable circular orbits (ISCOs). The local maxima of the effective potentials  $V_\sigma^+$  mean unstable circular orbits, which satisfy Eq. (59) and

$$\frac{d^2 V_\sigma^+}{dr^2} < 0. \quad (61)$$

We focus on the radial motions of charged particles in the quintessence field with  $-1 < \omega_q < -1/3$  and  $\alpha_q > 0$ . Since the effects of parameters  $a$ ,  $L$ ,  $Q$  and  $Q^*$  on the charged particle dynamics have been discussed in some references (e.g., [50,51]), the parameters  $b_c$ ,  $\alpha_q$ ,  $\omega_q$  and  $\sigma$  how to affect the radial effective potentials are mainly considered in Fig. 1. The graph at the equatorial plane  $\sigma = \pi/2$  in Fig. 1(a) shifts to the observer at infinity as the cloud strings parameter  $b_c$  increases. In this case, the energy decreases and the gravity from the black hole is weakened. This fact can be explained simply and intuitively in terms of the second term on line 1 of Eq. (39). The term  $\Psi = -(r^2 + a^2)^2(Q^*r/\Sigma - E)^2/(2\Sigma\Delta_r)$  gives gravitational effects to the charged particles. It is clear that  $\Delta_r$  is a decreasing function of  $b_c$ , and  $\Psi$  is, too. This implies that the gravity from the black hole becomes small as  $b_c$  increases. Therefore,  $V^+$  is a decreasing function of  $b_c$ . When the cloud strings parameter  $b_c$  increases in Table I, the graph going away the black hole leads to increasing the radius of ISCO at the equatorial plane, but decreasing the radius of SCO. Here, the ISCOs and SCOs are considered under the condition  $0 < V^+ < 1$  as well as the condition (60). The energy also decreases with an increase of the positive quintessence parameter  $\alpha_q$  in Fig. 1(b). However, the energy increases with the negative quintessential state parameter  $\omega_q$  increasing in Fig. 1(c). These results are because  $\Delta_r$  is a decreasing function of  $\alpha_q$  ( $> 0$ ) but an increasing function of  $\omega_q$ . The radii of ISCOs in Table I get larger when  $\alpha_q$  and  $\omega_q$  increase. An increase of  $\omega_q$  enlarges the radius of SCO, while that of  $\alpha_q$  diminishes the radius of SCO. Fig. 1(d) describes that the shape of the effective potential depends on the plane parameter  $\sigma$ . The potential decreases as  $\sigma$  increases. This result can be seen clearly from Eq. (58). Eq. (58) is rewritten as  $V^+ = -C_\sigma/(B + \sqrt{B^2 - A_\sigma C_\sigma})$ . Because  $C_\sigma$  is an increasing function of  $\sigma$  and  $A_\sigma$  is a decreasing function of  $\sigma$ ,  $V^+$  is a decreasing function of  $\sigma$ . An increase of  $\sigma$  results in decreasing the radii of SCOs and ISCOs.

In short, the main results concluded from Fig. 1 and Table I are given as follows. When anyone of the three parameters  $b_c$ ,  $\alpha_q > 0$  and  $\sigma \in (0, \frac{\pi}{2}]$  increases, the potential (or energy) decreases, whereas the potential increases with  $\omega_q < 0$  increasing. The radii of SCOs decrease as the four parameters increase. The radii of ISCOs gets larger with  $b_c$  and  $\alpha_q > 0$  increasing, but smaller with  $\omega_q$  and  $\sigma$  increasing.

Fig. 2 plots three SCOs and ISCOs at the planes  $\sigma = \pi/2$ ,  $\pi/4$  and  $\pi/6$  for the other parameters considered in Fig. 1(d). Here, an eighth- and ninth-order Runge-Kutta-Fehlberg integrator (RKF89) with adaptive step

sizes is applied to solve the canonical equations of the Hamiltonian (39). This integrator can give an order of  $10^{-12}$  to the Hamiltonian error  $\Delta H = H + 1/2$  when the integration time  $\tau = 10^5$ . These orbits still remain circular and stable in the three-dimensional configuration with  $x = r \sin \theta \cos \phi$ ,  $y = r \sin \theta \sin \phi$  and  $z = r \cos \theta$  during the integration time. Thus, the SCOs and ISCOs can exist not only in the equatorial plane but also in the non-equatorial planes.

#### D. Effective potentials and stable spherical orbits in the three-dimensional space

If  $K$  does not satisfy Eq. (57) with  $p_\theta = 0$  but is freely given and satisfies Eq. (44) with  $p_\theta \neq 0$ ,  $E^\pm$  in Eq. (49) are radial effective potentials in the three-dimensional space. The effective potentials are functions of separation  $r$  and depend on parameters  $a$ ,  $L$ ,  $K$ ,  $Q$ ,  $Q^*$ ,  $b_c$ ,  $\alpha_q$  and  $\omega_q$ .

The local extrema of the effective potentials  $E^+$  are spherical orbits with constant radii  $r$ . The spherical orbits should satisfy the condition

$$\frac{dE^+}{dr} = 0, \quad (62)$$

but do not always satisfy the condition  $\Theta(\theta) = 0$  for any time. The spherical orbits must be unstable in the unbound case of  $E^+ > 1$ . In the bound case of  $0 < E^+ < 1$ , the spherical orbits may either be stable or unstable. They are stable under perturbations in the radial direction if

$$\frac{d^2 E^+}{dr^2} \geq 0. \quad (63)$$

Eqs. (49), (62) and (63) are the conditions for the existence of the stable spherical orbits (SSOs). The equality symbol “=” in Eq. (63) corresponds to the marginally stable spherical orbits (MSSOs). In fact, the conditions for the SSOs are equivalent to the following conditions

$$\Re(r) = \frac{d\Re(r)}{dr} = 0, \quad \frac{d^2 \Re(r)}{dr^2} \leq 0, \quad (64)$$

which were considered in the existing publications [20,24]. All stable (or unstable) spherical orbits are of course confined to the ranges  $\theta \in [\vartheta, \pi - \vartheta]$  or  $\theta \in (0, \zeta] \cup [\pi - \zeta, \pi)$ . In particular, the conditions for the spherical orbits covering whole the range of the latitudinal coordinate are given in the above two cases. For  $L \neq 0$ , the spherical orbits do not cover whole the range of the latitudinal coordinate.

Fig. 3 describes the three-dimensional effective potentials  $E^+$ , which correspond to the parameters for the two-dimensional effective potentials  $V^+$  in Fig. 1 but  $\sigma$  gives place to  $K$ . The dependence of the three-dimensional potentials  $E^+$  on each of the three parameters  $b_c$ ,  $\alpha_q$  and  $\omega_q$  is in agreement with that of the two-dimensional potentials  $V^+$ . Unlike the dependence of  $V^+$  on  $\sigma$  in Fig.

2(d),  $E^+$  increases with an increase of  $K$  in Fig. 3(d). The reason is that  $E^+$  in Eq. (49) is an increase function of  $K$ . The impacts of the parameters  $b_c$ ,  $\alpha_q$  and  $\omega_q$  on the radii of SSOs and MSSOs in Table II are similar to those of SCOs and ISCOs in Table I. The radii of SSO and MSSO in Table II increase when the parameter  $K$  increases. Three spherical orbits and marginally spherical orbits are shown in Fig. 4. When the integration time reaches  $\tau = 10^5$ , these spherical orbits still remain stable.

There are other notable points in Table II. The presence of negative angular momenta  $L$  for some of the MSSOs means that of retrograde orbits moving against the black hole's rotation [23]. However, positive angular momenta  $L$  correspond to prograde orbits moving in the same direction as the black hole's rotation. In addition to these positive and negative angular momenta, vanishing angular momenta  $L = 0$  are also possible. For the case of zero angular momenta, stable spherical orbits and marginally stable spherical orbits cover whole the range of the latitudinal coordinate and reach the symmetry axis at  $\theta = 0$ , as shown in Fig. 5. Such spherical orbits are called as the polar spherical orbits [28]. However, the stable circular orbits are difficultly present for vanishing angular momentum  $L = 0$ . Why do the stable spherical orbits exist in the case of  $L = 0$ ? Why do the stable circular orbits not exist? The reason is that  $K$  does not satisfy Eq. (57) and is freely given for the stable spherical orbits, but must satisfy Eq. (57) and is not freely given for the stable circular orbits.

#### IV. CONCLUSIONS

We analytically show the integrability of the dynamics of charged particles moving around the Kerr-Newman black hole surrounded by cloud strings, quintessence and electromagnetic field. This integrability is due to the existence of a fourth constant of motion like the Carter constant. If a nonvanishing cosmological constant is included in the Kerr-Newman spacetime, then the fourth constant is absent.

Because of the presence of the fourth motion constant and the axial-symmetry of the spacetime, radial effective potentials and stable circular orbits in two-dimensional planes involving the equatorial plane and other nonequatorial planes can be present. The dynamical parameters play important roles in changing the graphs of the effective potentials. In addition, variations of these parameters affect the presence or absence of stable circular orbits and innermost stable circular orbits, and they also affect the radii of the stable circular orbits and innermost stable circular orbits. When each of the cloud strings parameter, quintessence parameter and plane parameter increases, the graph of effective potential shifts to the observer at infinity and the effective potential decreases. However, the graph of effective potential goes toward the black hole and the effective potential increases

as the quintessential state parameter increases. The radii of stable circular orbits decrease. The radii of the innermost stable circular orbits excluding those for the plane parameter and the quintessential state parameter increase. The changes of these parameters exert more influences on those of the radii of the stable circular orbits, but minor influences on those of the radii of the innermost stable circular orbits. Numerical tests show that the stable circular orbits and innermost stable circular orbits can exist not only in the equatorial plane but also in the non-equatorial planes.

On the other hand, the presence of the Carter-like constant and the axial-symmetry of the spacetime also gives a chance to the existence of radial effective potentials and stable spherical orbits in the three-dimensional space. The three-dimensional potential depending on each of the cloud strings parameter, quintessential state parameter and quintessence parameter is similar to the two-dimensional potential. The three-dimensional potential increases with an increase of the fourth motion constant. The radii of stable spherical orbits and marginally stable spherical orbits varying with the cloud strings parameter, quintessential state parameter and quintessence parameter is consistent with those of stable circular orbits and innermost stable circular orbits varying with these parameters. The radii of stable spherical orbits

and marginally stable spherical orbits increase when the Carter-like constant increases. The existence of some stable spherical orbits and marginally stable spherical orbits are numerically confirmed. In particular, some stable spherical orbits or marginally stable spherical orbits with vanishing angular momenta for covering whole the range of the latitudinal coordinate can also be found.

In sum, the Carter-like constant and the axial-symmetry of the spacetime can ensure the presence of stable circular orbits in two-dimensional nonequatorial planes and stable spherical orbits in the three-dimensional space if a vanishing cosmological constant appears in the Hamiltonian (30). Neither the stable circular orbits in nonequatorial planes nor the stable spherical orbits exist for a nonvanishing cosmological constant.

### Acknowledgments

The authors are very grateful to the referee for valuable comments and suggestions. This research was supported by the National Natural Science Foundation of China (Grant No. 11973020) and the Natural Science Foundation of Guangxi (Grant No. 2019JJD110006).

- 
- [1] S. Perlmutter et al. [Supernova Cosmology Project Collaboration], *Astrophys. J.* **517**, 565 (1999).
  - [2] V.V. Kiselev, *Class. Quantum Gravity* **20**, 1187 (2003).
  - [3] S. Hellerman, N. Kaloper, and L. Susskind, *JHEP* **0106**, 003 (2001).
  - [4] P.J. Steinhardt, L. Wang, and I. Zlatev, *Phys. Rev. D* **59**, 123504 (1999).
  - [5] L. Wang, R. Caldwell, J. Ostriker, and P.J. Steinhardt, *Astron. J.* **530**, 17 (2000).
  - [6] S. Tsujikawa, *Class. Quantum Gravity* **30**, 214003 (2013).
  - [7] I. Hussaina and S. Alib, *Eur. Phys. J. Plus* **131**, 275 (2016).
  - [8] P. S. Letelier, *Phys. Rev. D* **20**, 1294 (1979).
  - [9] S. Kar, *Phys. Rev. D* **55**, 4872 (1997).
  - [10] M.M. Dias e Costa, J.M. Toledo, and V.B. Bezerra, *Int. J. Mod. Phys. D* **28**, 1950074 (2019).
  - [11] J.M. Toledo and V.B. Bezerra, *Int. J. Mod. Phys. D* **1950023** (2019).
  - [12] E.T. Newman and A. Janis, *J. Math. Phys.* **6**, 915 (1965).
  - [13] S.G. Ghosh, *Eur. Phys. J. C* **76**, 222 (2016).
  - [14] J. Schee and Z. Stuchlík, *Eur. Phys. J. C* **76**, 643 (2016).
  - [15] T. Oteev, A. Abdujabbarov, and Z. Stuchlík, *Astrophys Space Sci* **361**, 269 (2016).
  - [16] B. Toshmatov, Z. Stuchlík, and B. Ahmedov, *Eur. Phys. J. Plus* **132**, 98 (2017).
  - [17] Z. Xu and J. Wang, *Phys. Rev. D* **95**, 064015 (2017).
  - [18] J.M. Toledo and V.B. Bezerra, *Gen. Relat. Gravit.* **52**, 34 (2020).
  - [19] B. Carter, *Phys. Rev.* **174**, 1559 (1968).
  - [20] E. Teo, *Gen. Rel. Grav.* **35**, 1909 (2003).
  - [21] P. V. P. Cunha and C. A. R. Herdeiro, *Phys. Rev. Lett.* **124**, 181101 (2020).
  - [22] D. C. Wilkins, *Phys. Rev. D* **5**, 814 (1972).
  - [23] M. Johnston and R. Ruffini, *Phys. Rev. D* **10**, 2324 (1974).
  - [24] E. Teo, *Gen. Rel. Grav.* **53**, 10 (2021).
  - [25] A. Tavlayan and B. Tekin, *Phys. Rev. D* **102**, 104036 (2020).
  - [26] T. Igata, H. Ishihara, and Y. Yasunishi, *Phys. Rev. D* **100**, 044058 (2019).
  - [27] D. Charbulák and Z. Stuchlík, *Eur. Phys. J. C* **78**, 879 (2018).
  - [28] D. Charbulák and Z. Stuchlík, *Eur. Phys. J. C* **77**, 897 (2017).
  - [29] Z. Stuchlík, D. Charbulák, and J. Schee, *Eur. Phys. J. C* **78**, 180 (2018).
  - [30] M. Bugden, *Gen. Rel. Grav.* **50**, 30 (2018).
  - [31] P. V. P. Cunha, C. A. R. Herdeiro, and E. Radu, *Phys. Rev. D* **96**, 024039 (2017).
  - [32] R. Narayan, M. D. Johnson, and C. F. Gammie, *Astrophys. J. Lett.* **885**, L33 (2019).
  - [33] S. E. Gralla, D. E. Holz, and R. M. Wald, *Phys. Rev. D* **100**, 024018 (2019).
  - [34] P. V. P. Cunha, E. Berti, and C. A. R. Herdeiro, *Phys. Rev. Lett.* **119**, 251102 (2017).
  - [35] P. V. P. Cunha, J. Grover, C. Herdeiro, E. Radu, H. Runarsson, and A. Wittig, *Phys. Rev. D* **94**, 104023 (2016).
  - [36] P. V. P. Cunha, C. A. R. Herdeiro, E. Radu, and H. F. Runarsson, *Phys. Rev. Lett.* **115**, 211102 (2015).
  - [37] P. Rana and A. Mangalam, *Class. Quant. Grav.* **36**,



- 045009 (2019).
- [38] L. C. Stein and N. Warburton, Phys. Rev. D **101**, 064007 (2020).
  - [39] G. Compère and A. Druart, Phys. Rev. D **101**, 084042 (2020).
  - [40] Z. Stuchlík and M. Kološ, Eur. Phys. J. C **76**, 32 (2016).
  - [41] A. Tursunov, Z. Stuchlík, and M. Kološ, Phys. Rev. D **93**, 084012 (2016).
  - [42] M. Takahashi and H. Koyama, Astrophys. J. **693**, 693, 472 (2009).
  - [43] O. Kopáček and V. Karas, Astrophys. J. **787**, 117 (2014).
  - [44] R. Panis, M. kološ, and Z. Stuchlík, Eur. Phys. C **79**, 479 (2019).
  - [45] O. Kopáček, V. Karas, J. Kovář, and Z. Stuchlík, Astrophys. J. **722**, 1240 (2010).
  - [46] O. Kopáček and V. Karas, Astrophys. J. **853**, 53 (2018).
  - [47] Z. Stuchlí, M. Kološ, J. Kovář, et al. Universe **6**, 6, 26 (2020).
  - [48] Y. Wang, W. Sun, F. Liu, and X. Wu, Astrophys. J. **907**, 66 (2021).
  - [49] E. Hackmann and H. Xu, Phys. Rev. D **87**, 124030 (2013).
  - [50] W. Sun, Y. Wang, F. Liu, and X. Wu, Eur. Phys. J. C **81**, 785 (2021).
  - [51] X. Sun, X. Wu, Y. Wang, C. Deng, B. Liu, and E. Liang, universe **7**, 410 (2021).

TABLE I: The radii  $R_C$  of SCOs and the radii  $R_I$  of ISCOs for the parameters considered in Fig. 1. The notation “-” means the absence of SCOs and ISCOs. The energies  $E$  of the SCOs are not arbitrarily given but are determined by  $R_C$ .  $E$  and the angular momentum  $L$  of the ISCOs are not arbitrarily given but are determined by  $R_I$ . The values are not given for  $E \geq 1$ . The radii  $R_C$  of SCOs decrease as anyone of the string cloud  $b_c$ , quintessence parameter  $\alpha_q$ , quintessential state parameter  $\omega_q$  and plane parameter  $\sigma$  increases. The radii  $R_I$  of ISCOs increase with the string cloud  $b_c$  and quintessence parameter  $\alpha_q$  increasing, but decrease with the quintessential state parameter  $\omega_q$  and plane parameter  $\sigma$  increasing.

Fig. 1(a)		$b_c$	0	0.05	0.1	0.15	0.2
SCO	$R_C$	10.15	8.26	-	-	-	-
	$E$	0.89	0.86	-	-	-	-
ISCO	$R_I$	6.33	6.72	7.17	7.67	8.25	
	$L$	3.71	3.93	4.18	4.45	4.78	
	$E$	0.88	0.86	0.83	0.8	0.78	
Fig. 1(b)		$\alpha_q$	0	0.1	0.2	0.3	0.4
SCO	$R_C$	12.13	9.84	-	-	-	-
	$E$	0.96	0.89	-	-	-	-
ISCO	$R_I$	5.67	6.4	7.37	8.72	10.77	
	$L$	3.38	3.75	4.22	4.85	5.7	
	$E$	0.93	0.88	0.82	0.75	0.68	
Fig. 1(c)		$\omega_q$	-0.35	-0.4	-0.45	-0.5	-0.55
SCO	$R_C$	11.94	12.14	12.65	14.06	-	-
	$E$	0.953	0.948	0.946	0.937	-	-
ISCO	$R_I$	5.73	5.76	5.8	5.88	6.06	
	$L$	3.42	3.41	3.39	3.38	3.34	
	$E$	0.94	0.93	0.92	0.91	0.90	
Fig. 1(d)		$\sigma$	$\pi/2$	$\pi/3$	$\pi/4$	$\pi/5$	$\pi/6$
SCO	$R_C$	11.93	17.5	28.3	44.71	60.66	
	$E$	0.95	0.96	0.97	0.98	0.99	
ISCO	$R_I$	5.73	5.77	5.82	5.87	5.89	
	$L$	3.41	2.97	2.62	2.03	1.73	
	$E$	0.89	0.90	0.91	0.92	0.93	

TABLE II: The radii  $R_S$  of SSOs and the radii  $R_M$  of MSSOs for the parameters considered in Figs. 3 and 5(a). The radii  $R_S$  of SSOs decrease when anyone of the string cloud  $b_c$ , quintessence parameter  $\alpha_q$ , and quintessential state parameter  $\omega_q$  increases, but increase with the increase of the Carter-like constant  $K$ . The radii  $R_M$  of MSSOs increase as the string cloud  $b_c$ , quintessence parameter  $\alpha_q$  and Carter-like constant  $K$  increase, whereas decrease with the increase of the quintessential state parameter  $\omega_q$ .

Fig. 3(a)	$b_c$	0	0.1	0.2	0.3	0.4
SSO	$R_S$	19.45	15.79	-	-	-
	$E$	0.91	0.85	-	-	-
MSSO	$R_M$	8.78	8.65	8.59	8.69	9.06
	$L$	-25.18	-13.37	0.64	18.16	41.76
	$E$	0.89	0.84	0.77	0.71	0.63
Fig. 3(b)	$\alpha_q$	0	0.1	0.2	0.3	0.4
SSO	$R_S$	18.48	15.79	-	-	-
	$E$	0.92	0.85	-	-	-
MSSO	$R_M$	8.62	8.65	8.76	9.06	9.78
	$L$	-24.95	-13.37	0.63	18.62	43.93
	$E$	0.91	0.84	0.77	0.69	0.60
Fig. 3(c)	$\omega_q$	-0.35	-0.4	-0.45	-0.5	-0.55
SSO	$R_S$	15.79	19.11	-	-	-
	$E$	0.85	0.81	-	-	-
MSSO	$R_M$	8.65	10.06	-	-	-
	$L$	-13.37	-15.99	-	-	-
	$E$	0.84	0.80	-	-	-
Fig. 3(d)	$K$	8	12	16	20	24
SSO	$R_S$	-	-	-	11.85	15.79
	$E$	-	-	-	0.84	0.85
MSSO	$R_M$	5.31	6.15	7	7.83	8.65
	$L$	22.8	14.74	5.93	-3.47	-13.37
	$E$	0.81	0.82	0.83	0.84	0.85
Fig. 5(a)	$K$	8	12	16	20	24
SSO	$R_S$	-	-	-	10.39	14.68
	$E$	-	-	-	0.84	0.85
MSSO	$R_M$	5.31	6.15	7	7.83	8.65
	$L$	22.8	14.74	5.93	-3.47	-13.37
	$E$	0.81	0.82	0.83	0.84	0.85

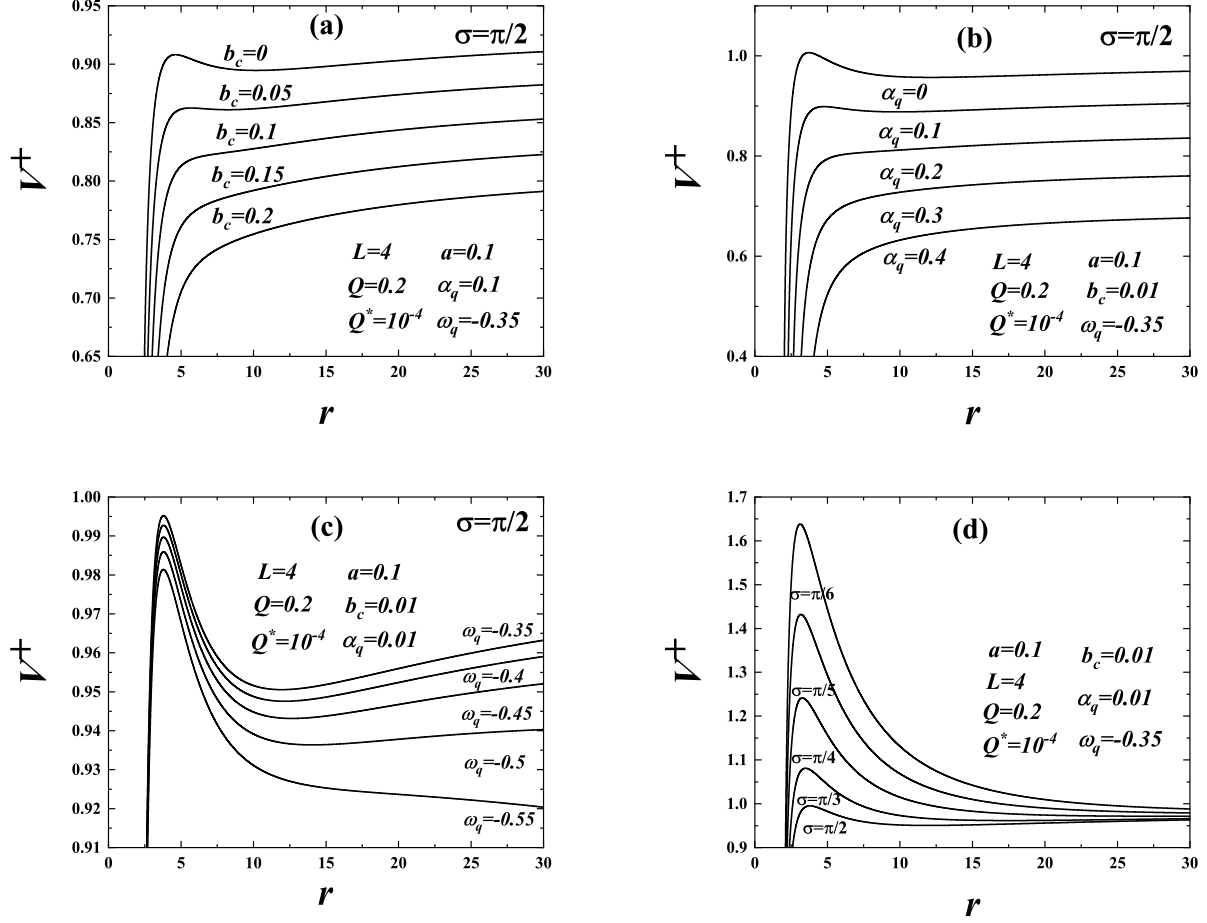


Fig. 1: Radial effective potentials  $V^+$  of Eq. (58) in two-dimensional planes  $\theta = \sigma$ . (a)-(c): They are plotted at the equatorial plane  $\sigma = \pi/2$ . (d): They are plotted in five planes  $\sigma = \pi/6, \pi/5, \pi/4, \pi/3$  and  $\pi/2$ . The impacts of the cloud strings parameter  $b_c$  in Eq. (10), quintessential state parameter  $\omega_q$  in Eq. (6), quintessence parameter  $\alpha_q$  in Eq. (7) and plane parameter  $\sigma$  on the effective potentials are shown in panels (a)-(d), respectively. The plane parameters  $\sigma$  satisfy Eq. (57) with  $p_\theta = 0$  and are constants. For a given separation  $r$ , the potentials (i.e., energies) decrease as each of the string cloud  $b_c$ , quintessence parameter  $\alpha_q$  and plane parameter  $\sigma$  increases, whereas increase when the quintessential state parameter  $\omega_q$  increases.

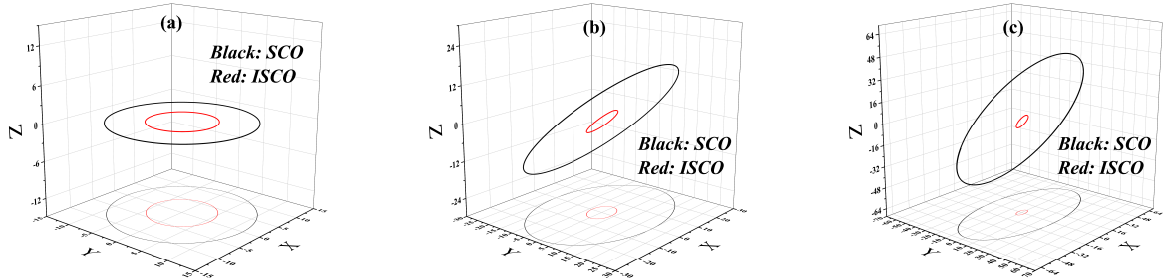


Fig. 2: Three examples of SCOs and ISCOS in two-dimensional planes. (a): The SCO colored Black on the plane  $\sigma = \pi/2$  has its radius  $r = 11.93$  and the ISCO colored Red has the radius  $r = 5.73$  and angular momentum  $L = 3.41$ . (b): The SCO colored Black on the plane  $\sigma = \pi/4$  has its radius  $r = 28.3$  and the ISCO colored Red has the radius  $r = 5.82$  and angular momentum  $L = 2.62$ . (c): The SCO colored Black on the plane  $\sigma = \pi/6$  has its radius  $r = 60.66$  and the ISCO colored Red has the radius  $r = 5.89$  and angular momentum  $L = 1.73$ . The plane parameters  $\sigma$  satisfy Eq. (57) with  $p_\theta = 0$  and are constants. The other parameters in each of the panels are the same as those of Fig. 1(d). The upper part of each panel corresponds to the practical trajectories, and the bottom part relates to projections of the practical trajectories. These orbits still remain circular and stable in the three-dimensional space  $XYZ$  when the integration time  $\tau = 10^5$ .

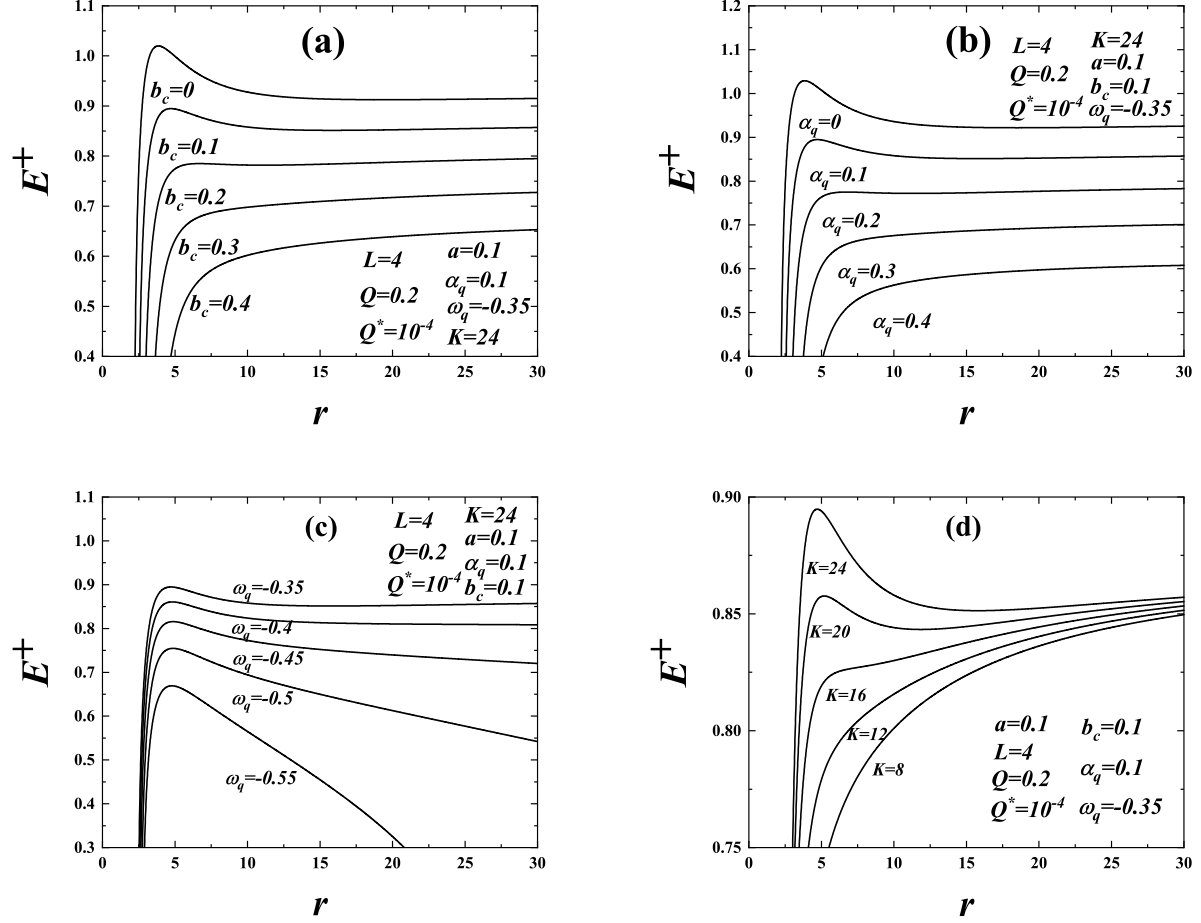


Fig. 3: Radial effective potentials  $E^+$  of Eq. (49) in the three-dimensional configuration. (a): The dependence of  $E^+$  on the cloud strings parameter  $b_c$  shows the decrease of  $E^+$  with the increase of  $b_c$ . (b): The dependence of  $E^+$  on the quintessence parameter  $\alpha_q$  describes the decrease of  $E^+$  with the increase of  $\alpha_q$ . (c): The dependence of  $E^+$  on the quintessential state parameter  $\omega_q$  indicates the increase of  $E^+$  with the increase of  $\omega_q$ . (d): The dependence of  $E^+$  on the Carter-like constant  $K$  exhibits the increase of  $E^+$  with the increase of  $K$ , where  $K$  does not satisfy Eq. (57) with  $p_\theta = 0$  but is freely given and satisfies Eq. (44) with  $p_\theta \neq 0$ .



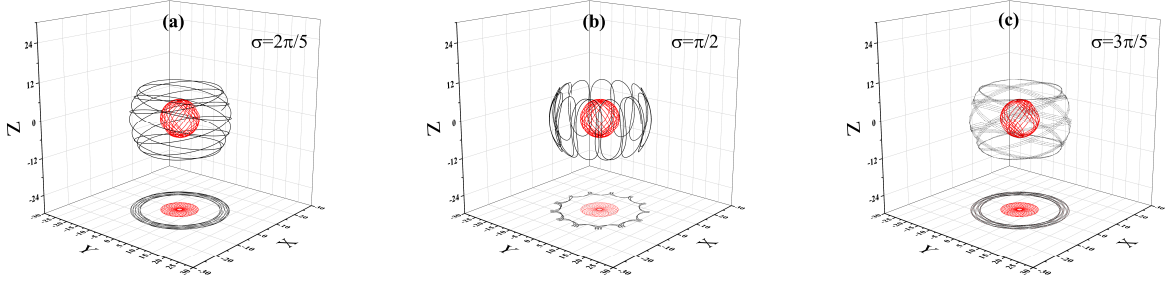


Fig. 4: Three examples of SSOs and MSSOs in the three-dimensional space. (a): The SSO colored Black has the initial values  $\sigma = 2\pi/5$  and  $p_\theta = 2.64$ , and the MSSO colored Red has the initial values  $\sigma = 2\pi/5$  and  $p_\theta = 2.46$ . (b): The SSO colored Black has the initial values  $\sigma = \pi/2$  and  $p_\theta = 2.94$ , and the MSSO colored Red has the initial values  $\sigma = \pi/2$  and  $p_\theta = 2.71$ . (c): The SSO colored Black has the initial values  $\sigma = 3\pi/5$  and  $p_\theta = 2.64$ , and the MSSO colored Red has the initial values  $\sigma = 3\pi/5$  and  $p_\theta = 2.46$ . In these panels, all SSOs have the radii  $R_S = 15.79$  and the Carter-like constant  $K = 24$ , and all MSSOs correspond to the radii  $R_M = 7.83$ , the angular momentum  $L = -3.47$  and the Carter-like constant  $K = 20$ . The other parameters are the same as those of Fig. 3(d). Unlike those in Figs. 1 and 2, the values of  $\sigma$  do not satisfy Eq. (57) with  $p_\theta = 0$  and are no longer constant plane parameters. In fact, the values of  $\sigma$  in the three panels, such as  $\sigma = 2\pi/5$  in panel (a), are only the initial values of  $\sigma$  but are not invariant with time. The upper part of each panel corresponds to the practical trajectories, and the bottom part relates to projections of the practical trajectories. These orbits still remain spherical and stable when the integration time  $\tau = 10^5$ .

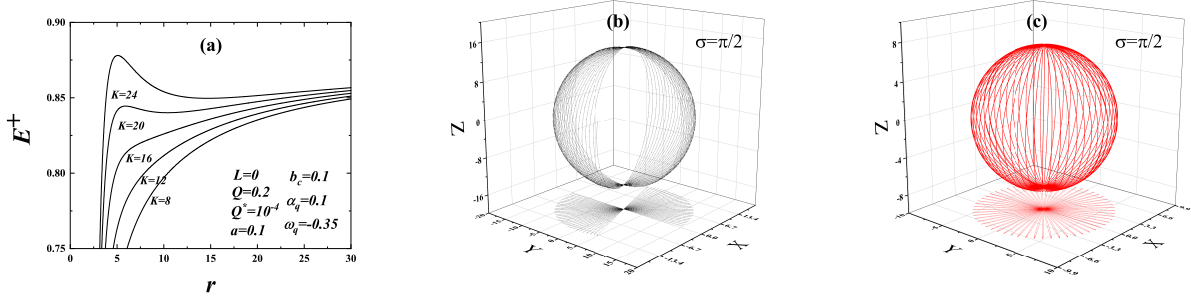


Fig. 5: (a): Relation between the Carter-like constant  $K$  and radial effective potential  $E^+$  with zero angular momentum  $L = 0$  in the three-dimensional configuration. The potential increases with  $K$  increasing, where  $K$  does not satisfy Eq. (57) with  $p_\theta = 0$  but is freely given and satisfies Eq. (44) with  $p_\theta \neq 0$ . (b): A stable spherical orbit with  $K = 24$ , the radius  $R_S = 14.68$  and the initial value  $p_\theta = 4.89$ . (c): A marginally stable spherical orbit with  $K = 18.54$ , the radius  $R_M = 7.53$  and the initial value  $p_\theta = 4.31$ . The other parameters of panels (b) and (c) are those of panel (a). Unlike those in Figs. 1 and 2, the values of  $\sigma$  do not satisfy Eq. (57) with  $p_\theta = 0$  and are no longer constant plane parameters. In fact,  $\sigma = \pi/2$  is only the initial value of  $\sigma$  but varies with time. The upper part of each panel corresponds to the practical trajectories, and the bottom part relates to projections of the practical trajectories. The two spherical orbits seem to have same sizes but have different radii:  $R_S = 14.68$  in panel (b) and  $R_M = 7.53$  in panel (c). These orbits with vanishing angular momenta for covering whole the range of the latitudinal coordinate in panels (b) and (c) still remain spherical and stable when the integration time  $\tau = 10^5$ .